

# Defect-Free, Highly Uniform Washable Transparent Electrodes Induced by Selective Light Irradiation

Zhaoyang Zhong, Kyoohee Woo,\* Inhyuk Kim, Hyuntae Kim, Pyeongsam Ko, Dongwoo Kang, Sin Kwon, Hyunchang Kim, Hongseok Youn, and Jooho Moon\*

A simple route to fabricate defect-free Ag-nanoparticle–carbon-nanotube composite-based high-resolution mesh flexible transparent conducting electrodes (FTCEs) is explored. In the selective photonic sintering-based patterning process, a highly soft rubber or thin plastic substrate is utilized to achieve close and uniform contact between the composite layer and photomask, with which uniform light irradiation can be obtained with diminished light diffraction. This well-controlled process results in developing a fine and uniform mesh pattern ( $\approx 12\ \mu\text{m}$ ). The mesh patternability is confirmed to be dependent on heat distribution in the selectively light-irradiated film and the pattern design for FTCE could be adopted for more precise patterns with desired performance. Moreover, using a very thin substrate could allow the mesh to be positioned closer to the strain-free neutral mechanical plane. Due to strong interfacial adhesion between the mesh pattern and substrate, the mesh FTCE could tolerate severe mechanical deformation without performance degradation. It is demonstrated that a transparent heater with fine mesh patterns on thin substrate can maintain stability after 100 repeated washing test cycles in which a variety of stress situations occurring in combination. The presented highly durable FTCE and simple fabrication processes may be widely adoptable for various flexible, large-area, and wearable optoelectronic devices.

systems.<sup>[1–7]</sup> Accordingly, their electronic components have evolved from rigid and bulky platforms to thin and flexible ones with high mechanical stability under severe structural deformation. For example, instead of the conventional indium tin oxide transparent electrodes commonly used for numerous optoelectronic devices, alternatives such as conducting polymers, carbon nanotubes (CNTs), graphene, metal nanowires, and their hybrids have been exploited for flexible transparent conducting electrodes (FTCEs).<sup>[8–16]</sup> Recently, the concept of using ultrathin and light-weight plastic electronics to achieve unprecedented mechanical stability has been explored, enabling practical demonstrations including artificial electronic skin and flexible solar cells.<sup>[17–20]</sup> Furthermore, there is a growing need to realize cost-effective, large-area, and large-scale production of flexible electronics. Therefore, instead of silicon- or glass-based conventional fabrications, various printing processes without the need for multiple manufacturing steps, the use of toxic etchants and rigid carrier substrate, and with the advantage of scalability have been

Human-friendly devices that are highly deformable, wearable, and portable are of increasing interest for various electronic applications such as displays, lighting, and photovoltaic


developed.<sup>[21–28]</sup> However, despite enormous efforts, they still suffer from difficulties in improving reliability, throughput, and pattern resolution. This poses a hurdle to the wide exploitation of printing methodologies as a replacement for the traditional technologies that currently dominate the electronics industry.

Among various efforts to resolve these issues,<sup>[29–32]</sup> we reported a selective light-induced patterning (SLIP) process for Ag nanoparticle (AgNP)–CNT composite-based highly flexible conductive patterns.<sup>[33]</sup> In this process, a significant difference in adhesion between the light-exposed and nonexposed regions with respect to the substrate could be induced using selective irradiation by intense pulsed light (IPL) through a photomask, followed by wiping out the nonirradiated part of the layer that has not strongly adhered to the underlying substrate. In this way, patterning could be easily accomplished. It was demonstrated that our SLIP process could be eco-friendly and compatible with scalable and rapid production, enabling flexible conductive patterns on top of heat-sensitive plastic substrates with less thermal shrinkage and without additional annealing processes. However, several bottlenecks such as variation in

Dr. Z. Zhong, I. Kim, Prof. J. Moon  
Department of Materials Science and Engineering  
Yonsei University  
50 Yonsei-ro, Seodaemun-gu, Seoul 03722, Republic of Korea  
E-mail: jmoon@yonsei.ac.kr

Dr. Z. Zhong, Dr. K. Woo, H. Kim, P. Ko, Dr. D. Kang,  
Dr. S. Kwon, Dr. H. Kim  
Advanced Manufacturing Systems Research Division  
Korea Institute of Machinery and Materials (KIMM)  
156 Gajeongbuk-ro, Yuseong-Gu, Daejeon 34103, Republic of Korea  
E-mail: khwoo@kimm.re.kr

P. Ko, Prof. H. Youn  
Department of Mechanical Engineering  
Hanbat National University  
Dongseodaero 125, Yuseong-gu, Daejeon 34158, Republic of Korea

 The ORCID identification number(s) for the author(s) of this article can be found under <https://doi.org/10.1002/sml.201800676>.

DOI: 10.1002/sml.201800676

pattern size and incomplete pattern generation over large-area substrates were often observed owing to irregularly distributed light intensity and augmented light diffraction caused by less intimate contact formation between a hard photomask and the composite layer to be patterned. In other words, to achieve highly reliable, fine patterns with high uniformity and fidelity, uniform light irradiation is essential to diminish random light diffraction by forming a narrow and uniform air gap between the conductive film and the photomask.

Herein, we propose a promising simple route to fabricate defect-free, AgNP–CNT composite-based high-resolution mesh FTCEs that can tolerate externally applied severe mechanical stimuli like washing tests in which a variety of stress situations such as rubbing, folding, and crumpling occur simultaneously in soapy water. Fine mesh-patterned FTCEs without defects and performance degradation under severe mechanical stress could be achieved by either inserting a highly soft rubber support or adopting a thin plastic substrate that could be easily deformed according to the contour of an arbitrarily shaped solid. **These strategies enable the formation intimate and uniform contact between the AgNP–CNT layer and the photomask, so as to allow uniform light irradiation with diminished irregular diffraction, leading to the development of fine and uniform mesh patterns. In addition, the use of a thin flexible substrate enables the fabricated FTCE to be located much closer to the zero-strain neutral plane, leading to a remarkable improvement in the mechanical flexibility.** The minimum resolution of the developed mesh patterns as a function of the IPL processing parameters and substrate thickness was investigated. As indicated by a simulation of the heat transfer in a selectively light-irradiated composite film, there was a strong correlation between heat conduction and patternability. We also successfully fabricated a fine-mesh-based ultraflexible and highly transparent heater as a proof-of-concept, revealing high stability against repeated washing tests. Our demonstration clearly proves its potential for use in various flexible and wearable electronic devices.

A uniform **AgNP–CNT composite film** of thickness  $\approx 600$  nm was prepared on a  $100\ \mu\text{m}$  thick polyethylene terephthalate (PET) substrate by spin-coating using an ink composed of a mixture of AgNPs and multiwalled CNTs (MWCNTs) (1.8 wt%). The detailed preparation procedure is described in the Experimental Section. It was then selectively exposed to IPL through a photomask with mesh patterns of  $20\ \mu\text{m}$  line width, followed by wiping out the nonirradiated part of the film, yielding AgNP–CNT-based mesh patterns. However, as shown in Figure S1a (Supporting Information), it was observed that some part of the lines were unseen, as indicated by red arrows, and narrowed the developed mesh pattern; a large deviation in the sheet resistance ( $R_s$ ) distribution was thus observed on the sample size of  $5\ \text{cm} \times 5\ \text{cm}$ . **These imperfections might be due to nonuniform light intensity caused by an uneven large air gap between the AgNP–CNT film and the hard mask.** To achieve uniform and conformal contact between the composite film and mask, a highly soft rubber sheet that could be easily deformed according to the surface of an arbitrarily shaped solid was placed underneath the coated composite film and the mask/composite film/rubber stack was compressed by a custom-built clamp, as illustrated in **Figure 1a**. When the stack was irradiated by IPL, the photonic energy was varied by

controlling the operating voltage (320, 330, 340, and 350 V) with a fixed exposure time of  $1000\ \mu\text{s}$  and the resultant mesh patterns were observed by field-emission scanning electron microscopy (FESEM), as shown in Figure 1b. At 320 V, well-defined mesh with lines as narrow as  $13\ \mu\text{m}$  and less deviation ( $\pm 0.55\ \mu\text{m}$ , the detailed calculation method was described in the Experimental Section) was achieved, exhibiting a low  $R_s$  value of  $8.92 \pm 0.26\ \Omega\ \text{sq}^{-1}$  and 95.05% transmittance ( $T$ ) at the wavelength of 550 nm. With the assistance of a rubber support allowing a negligible air gap between the coated layer and the mask, highly uniform mesh patterns could be developed with fewer defects, as shown in Figure S1b (Supporting Information). As the voltage increased to 350 V, the line width broadened to  $24\ \mu\text{m}$  and the optoelectrical performance of the developed mesh was measured to be  $3.89\ \Omega\ \text{sq}^{-1}$  at 92.65%  $T$ .

In this rubber-assisted patterning route, the air gap between the coated layer and the mask was near zero, such that the effect of light diffraction on the patterning shape and resolution could be negligible. However, narrower or broader line pattern than that of photomask could be developed, as shown in Figure 1b. In addition, the abnormal widening at four-way intersection of the mesh was also observed in Figure 1c. To clarify the reason for this, the heat behavior in selectively IPL-irradiated AgNP–CNT film was simulated using the ANSYS simulation tool under simplified boundary conditions (see the Experimental Section in details). As shown in the temperature distribution contour in Figure 1c, after instant IPL irradiation, a high temperature rise was observed at the central part of the irradiated area (defined by the dotted lines) and the intensity of heat energy decreased toward the edge of the line pattern, as indicated by the yellow/green color. The heat generated at the edge of an irradiated area was easily transferred to an adjacent nonirradiated area. However, the heat energy in the center of the irradiated area could be not well-spread to the side areas, and thus the heat was retained in the center of the line pattern. In other words, the variation of heat energy was present according to center or edge of line. When the heat energy of the edge of the pattern was lower than the threshold energy for the fusion between the AgNP–CNT film and the PET substrate, a narrower pattern than the aperture size of the mask could be developed. On the contrary, if heat energy at edge was higher than the energy for fusion by applying high voltage, broader line could be also generated.

Moreover, at the intersection of the mesh lines where the heat was developed on four different sides, the heat could be concentrated because of the resistance to heat transfer to the surrounding. By this excessive heat, the much wider pattern at the cross junction of the mesh was generated. It was noted that this widening could cause performance deterioration such as loss of transmittance. To solve this widening, the mesh photomask design was changed from square type to the honeycomb type of three-way intersection, which could be advantageous to suppress the concentration of heat energy. Less heat was focused on three-way intersection of honeycomb, so that the widening at intersection of the developed honeycomb mesh could be considerably reduced as shown in Figure 1d. As a result, the transmittance ( $\approx 89.5\%$ ) of the conductive mesh electrode derived by the honeycomb-shaped photomask was measured to be similar to that (90%) of photomask and higher than the square-shaped

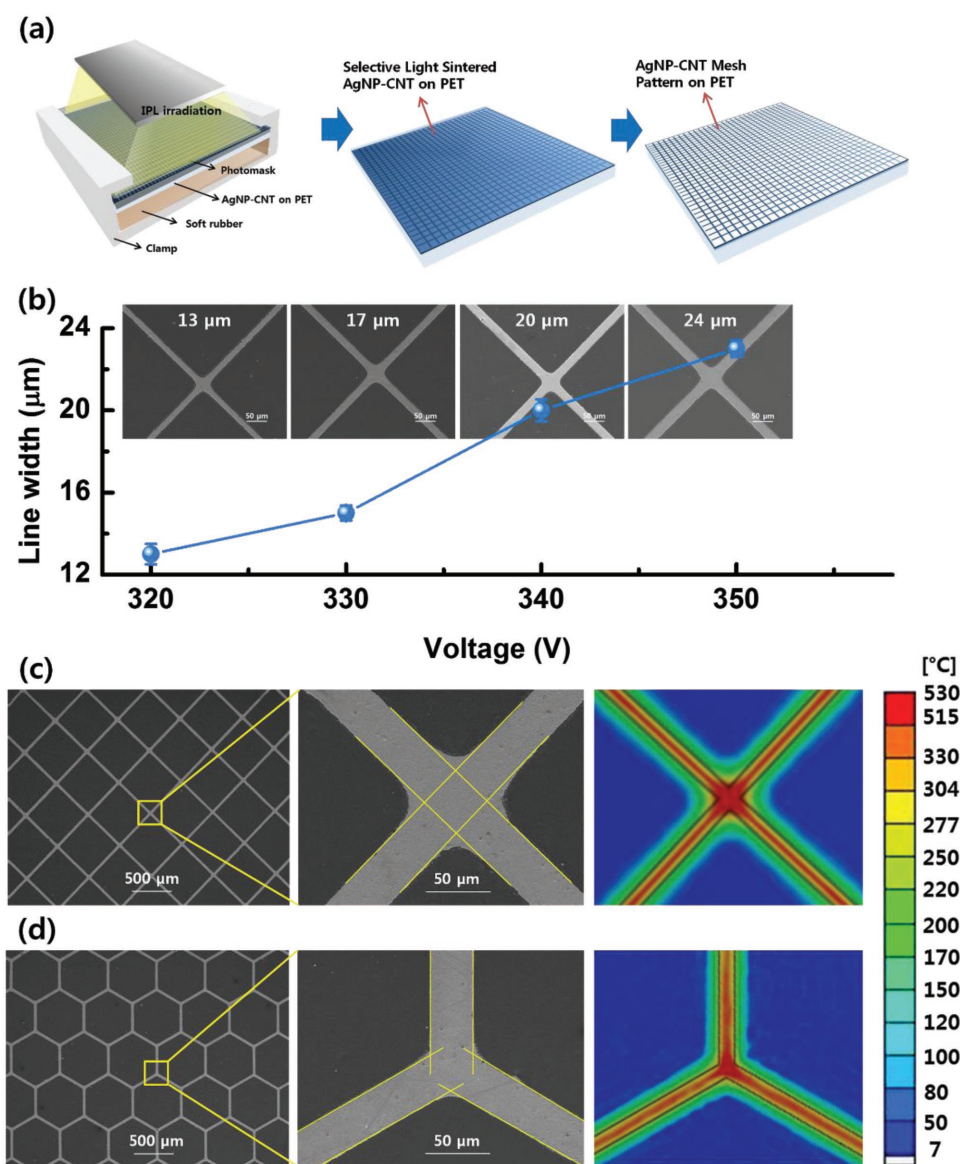


**Figure 1.** a) Schematic diagram of a highly soft rubber-assisted SLIP method for fabricating fine and uniform AgNP–CNT mesh. b) Line width variation of AgNP–CNT mesh patterns as a function of operation voltage of IPL. The inset shows FESEM images for the developed mesh patterns. c) The microscopic image for the widened pattern at the cross intersection of the developed square type mesh. Widening seemed to closely correlate with the heat distribution, as deduced from simulation result in which the heat generated in the selectively IPL-irradiated film is concentrated on four-way intersection of the square mesh when using the photomask of square type mesh. d) The microscopic image for the honeycomb mesh pattern. Temperature distribution derived from simulation also shows that the concentration of heat energy at three-way intersection of honeycomb mesh is suppressed so that the widened cross intersection was not developed in the patterned mesh electrode.

mesh electrode ( $\approx 88\%$ ) as shown in Figure S2 (Supporting Information). It was confirmed that the predominant factor affecting the patternability in our patterning process could be the behavior of heat conduction/dissipation and the geometry of photomask for FTCE could be controlled for more precise patterns with desired performance.

Although the highly soft-rubber-assisted SLIP process enables the fabrication of uniform and fine mesh patterns, contamination from the direct contact between the as-coated composite film and photomask may occur. Furthermore, if this SLIP process were adapted to roll-to-roll (R2R) processing (i.e.,

R2R-based coating-selective light-irradiation wiping), it would be difficult to use a rubber support for continuous R2R-based patterning. Instead, we excoagulated a reverse side-SLIP (R-SLIP) process, as depicted in Figure 2a. The AgNP–CNT coated film was turned upside down and then the photomask was directly placed on the backside of the substrate. It was considered that a thinner substrate could be more desirable to obtain a uniform and high-resolution mesh pattern, because the thickness of the substrate literally defines the distance between the coated layer and the photomask. Therefore, using a thinner substrate allows a narrower gap between the coated film and the mask.

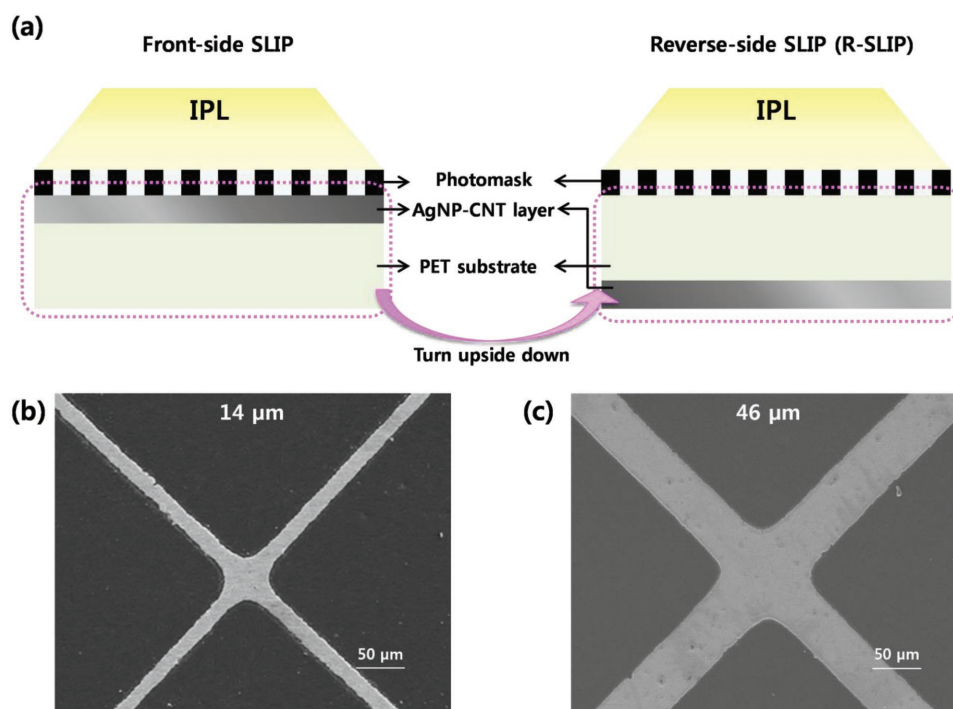


**Figure 2.** a) Schematic diagram showing a comparison between the front-side and reverse-side SLIP methods. The reverse-side-SLIP-derived mesh patterns on substrates of thickness b) 10  $\mu\text{m}$  and c) 100  $\mu\text{m}$ . The selective IPL irradiation was performed at 320 V for 1000  $\mu\text{s}$ .

Moreover, a thinner substrate with a lower flexural rigidity better fits to conformal contact with the surface of the hard mask, as compared to the stiffer and thicker substrate. In this regard, instead of a soft rubber, a thin substrate can nearly eliminate the air gap between the composite film and mask, reducing the light diffraction and enabling the development of uniform fine mesh pattern by the R-SLIP process.

Figure 2b shows an FESEM image of the mesh pattern with  $\approx 14 \mu\text{m}$  line width that was fabricated on a very thin ( $\approx 10 \mu\text{m}$ ) substrate via the R-SLIP process using a photo-mask with a mesh of 20  $\mu\text{m}$  line width and without an aid of a rubber support. The pattern resolution was similar to that of a rubber-assisted front side-SLIP process. A mesh pattern with a uniform  $R_s$  distribution was demonstrated, as shown in Figure S3 (Supporting Information), which is similar to the result of a rubber-assisted process (Figure S1b, Supporting Information). To confirm the effect of substrate thickness on pattern resolution, a 100  $\mu\text{m}$  thick substrate was also evaluated. In this case, even though the rubber was used as well, the minimum line width to be developed was measured as  $\approx 46 \mu\text{m}$  (Figure 2c), which is due to the increased light diffraction coming from the wider gap (i.e., thicker substrate) between the mask and the composite layer. This observation implies that the R-SLIP process could be effective in the fabrication of high-quality mesh-based FTCEs on a thin flexible substrate, while avoiding practical problems such as mask contamination and incompatibility issues regarding R2R processing.

The electrical properties of the mesh-type FTCEs without loss of  $T$  could be easily controlled by varying the thickness of the mesh pattern. Therefore, mesh patterns with various thicknesses (320, 600, 1200, and 1700 nm) were developed on

thin ( $\approx 10 \mu\text{m}$ ) PET substrates by controlling the spin-coating conditions and their properties were investigated, as shown in Figure 3a as well as Table 1. As the film became thicker from 320 to 1700 nm, the  $R_s$  values of the developed mesh patterns significantly decreased from 17.03 to 1.47  $\Omega \text{ sq}^{-1}$ , whereas  $T$  slightly decreased from 95.54% to 94.12% owing to the slightly increased line width. To evaluate the optoelectrical performance of the fabricated mesh FTCEs, the figure of merit (FoM) defined by Haacke<sup>[34]</sup> was calculated as follows:

$$\text{FoM} = T^{10}/R_s \quad (1)$$

The FoM of our meshes as well as the corresponding patterning resolution are summarized in Table 1, along with the comparison data of related mesh electrodes prepared by various solution-based printing technologies such as inkjet printing, screen printing, and reverse-offset printing.<sup>[35–38]</sup> Through our R-SLIP method, the resolution of  $\approx 12 \mu\text{m}$  could be achieved, which is remarkably high as compared to other methods with the resolution of 20–160  $\mu\text{m}$ . In addition, our FTCE with mesh thickness of 1700 nm showed a much higher FoM than the meshes fabricated by most of the other technologies. Although the FOM of the mesh fabricated by screen printing was higher than the present result, its resolution ( $\approx 160 \mu\text{m}$ ) was much lower. This indicates that our mesh FTCEs fabricated by the R-SLIP method exhibit outstanding performance, with high resolution as well as superior optoelectrical properties.

A more important advantage of using a thin substrate is manifested by the dramatically improved mechanical flexibility. In a homogeneous bent film, as illustrated in Figure S4



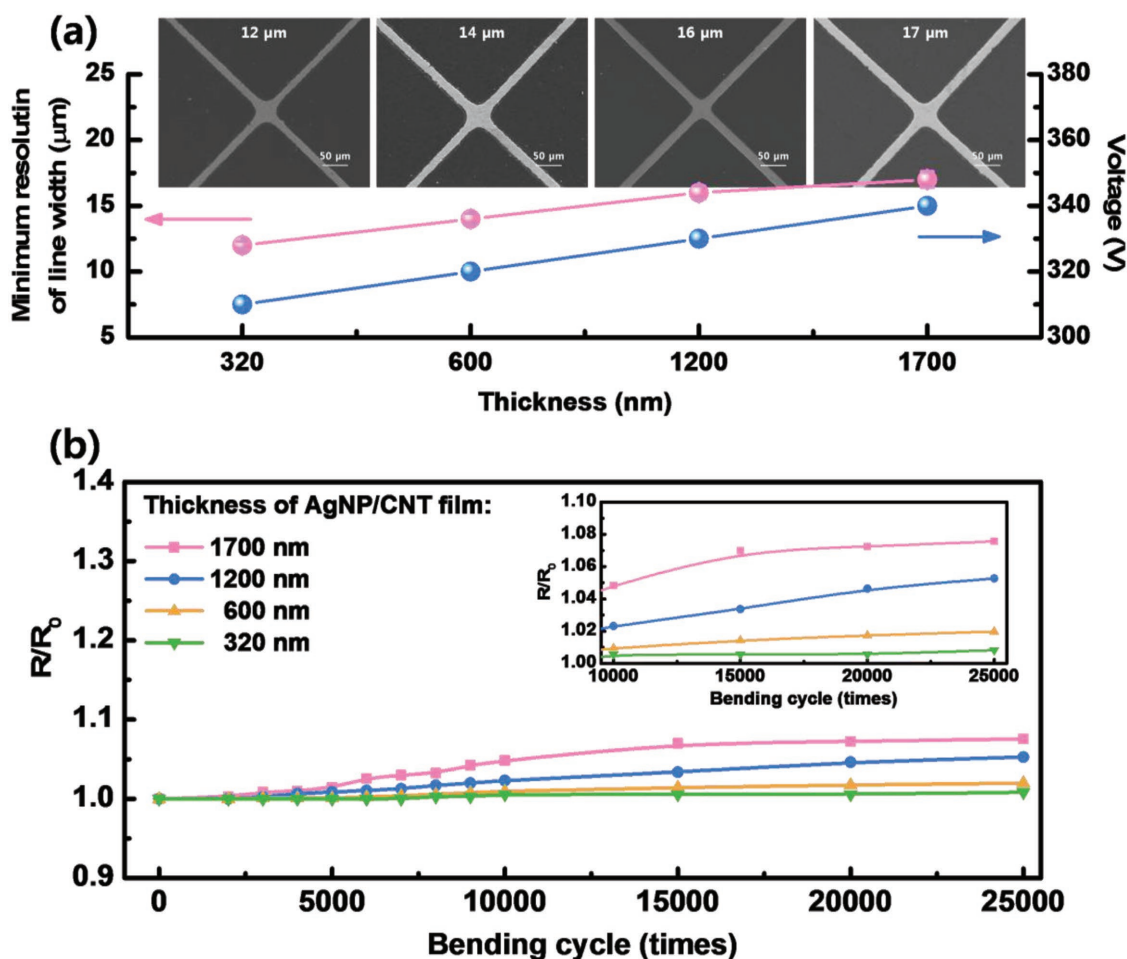


**Figure 3.** a) Variation in the minimum resolution of line width and IPL operating voltage as a function of AgNP-CNT thickness (320, 600, 1200, and 1700 nm). FESEM images for developed mesh patterns with various thicknesses are shown in the insets. b) Electrical resistivity change ( $R/R_0$ ) depending on the thickness of the AgNP-CNT mesh FTCE. Bending test was performed under 25 000 bending cycles at a fixed radius of 1 mm. The inset shows an enlarged plot of the resistivity change after 10 000 bending cycles.

(Supporting Information), the geometrical central plane in the cross-sectional view is not under stress, which is defined as a neutral plane. Therefore, the stress ( $\sigma$ ) of the observed plane could be increased with increasing distance ( $y$ ) to the neutral plane, as expressed by:

$$\sigma = -E\gamma/\rho \quad (2)$$

where  $E$  and  $\rho$  denote the Young's modulus and the radius of bending curvature, respectively. Thus, the usage of a thinner substrate can position the mesh FTCEs much closer to the stress-free neutral plane, thereby drastically improving their flexibility.<sup>[17,39]</sup> The mechanical flexibility of the mesh FTCEs with varied AgNP-CNT film thicknesses was evaluated using a custom-built automatic bending tester, as shown in Figure 3b.

**Table 1.** Comparison of the characteristics of the mesh-patterned FTCEs fabricated by various solution-based processes.

| Solution-based process    | Minimum line width [μm] | Film thickness [nm] | $R_s$ [ $\Omega$ sq <sup>-1</sup> ] | $T$ [%] | FoM [ $\Omega^{-1}$ ] | Reference |
|---------------------------|-------------------------|---------------------|-------------------------------------|---------|-----------------------|-----------|
| Reverse-side SLIP process | 12                      | 320                 | 17.0                                | 95.5    | 0.037                 | This work |
|                           | 14                      | 600                 | 8.1                                 | 94.8    | 0.072                 |           |
|                           | 16                      | 1200                | 3.7                                 | 94.3    | 0.150                 |           |
|                           | 17                      | 1700                | 1.5                                 | 94.1    | 0.371                 |           |
| Inkjet printing           | 50                      | 200                 | 10.3                                | 73.0    | 0.004                 | [35]      |
| Screen printing           | 160                     | 2000                | 1.0                                 | 93.0    | 0.484                 | [36]      |
| Reverse-offset printing   | 20                      | 200                 | 12.9                                | 85.6    | 0.016                 | [37]      |
| Gravure-offset printing   | 32                      | 1300                | 9                                   | 93.5    | 0.057                 | [38]      |

The bending test was performed under 25 000 bending cycles at the bending radius of  $\approx 1$  mm. As the thickness increased, the electrical resistivity change ( $R/R_0$ ) increased slightly. However, after 25 000 cycles, the  $R/R_0$  value of the thickest (1700 nm) mesh was observed to remain below  $\approx 1.08$ , and the resistance of the other thinner samples remained almost constant. As described in previous work,<sup>[33]</sup> high flexibility could be achieved owing to the addition of CNTs, which acted as conducting bridges in the AgNP film. However, in this case, the superior flexibility could not be only due to the CNTs. It is considered to be more significantly caused by the strong adhesion between the contacting surfaces of the mesh and the substrate, as well as the benefit of a thin substrate. Mechanical failures such as fracture of the pattern and interfacial delamination could be prevented by strong adhesion. As shown in Figure S5a (Supporting Information), the adhesion property of the IPL-irradiated AgNP–CNT film was measured according to ASTM D3359-17<sup>[40]</sup> as the standard method. The IPL-irradiated AgNP–CNT film was cut into 100 subzones. Then adhesive tape (Scotch 3M) was attached on the surface of the film and pressed firmly for 90 s. Afterward, the tape was detached rapidly and the removed area of the film was inspected. As seen in Figure S5b (Supporting Information), there was no area to be peeled after tape test, indicating that adhesion class of our

IPL-irradiated film belonged to the strongest class of 5B. In addition, R-SLIP method derived AgNP–CNT mesh electrode also exhibited excellent adhesion property after 100 cycles tape test as shown in Figure S5c (Supporting Information). Furthermore, the use of a thin substrate allows the mesh FTCE to be positioned closer to the strain-free neutral mechanical plane, so that less bending-induced strain is developed in the mesh FTCE and the conductive pattern remains stable against severe mechanical deformation.

To demonstrate the usefulness of our mesh FTCE and its process, an ultraflexible transparent conductive heater (TCH) with the dimensions of  $60 \times 60$  mm<sup>2</sup> was successfully fabricated on 10  $\mu$ m thick PET substrate using the R-SLIP process. The prepared TCH was based on the AgNP–CNT mesh with 14  $\mu$ m line width and its resistivity was measured to be 21.9  $\Omega$ . To verify whether our TCH could survive under harsh environments that could occur in real life or not, it was hand-washed, as shown in Figure 4a. To mimic a realistic scenario, detergent was dissolved in water and then TCH was exposed to a variety of stress situations such as rubbing, folding, and crumpling in the prepared solution. After being washed for  $\approx 1$  min and then rinsed, it was confirmed that the resistivity of the TCH was almost constant. Before and after washing, distinguishable cracks or damages were not observed on the surface

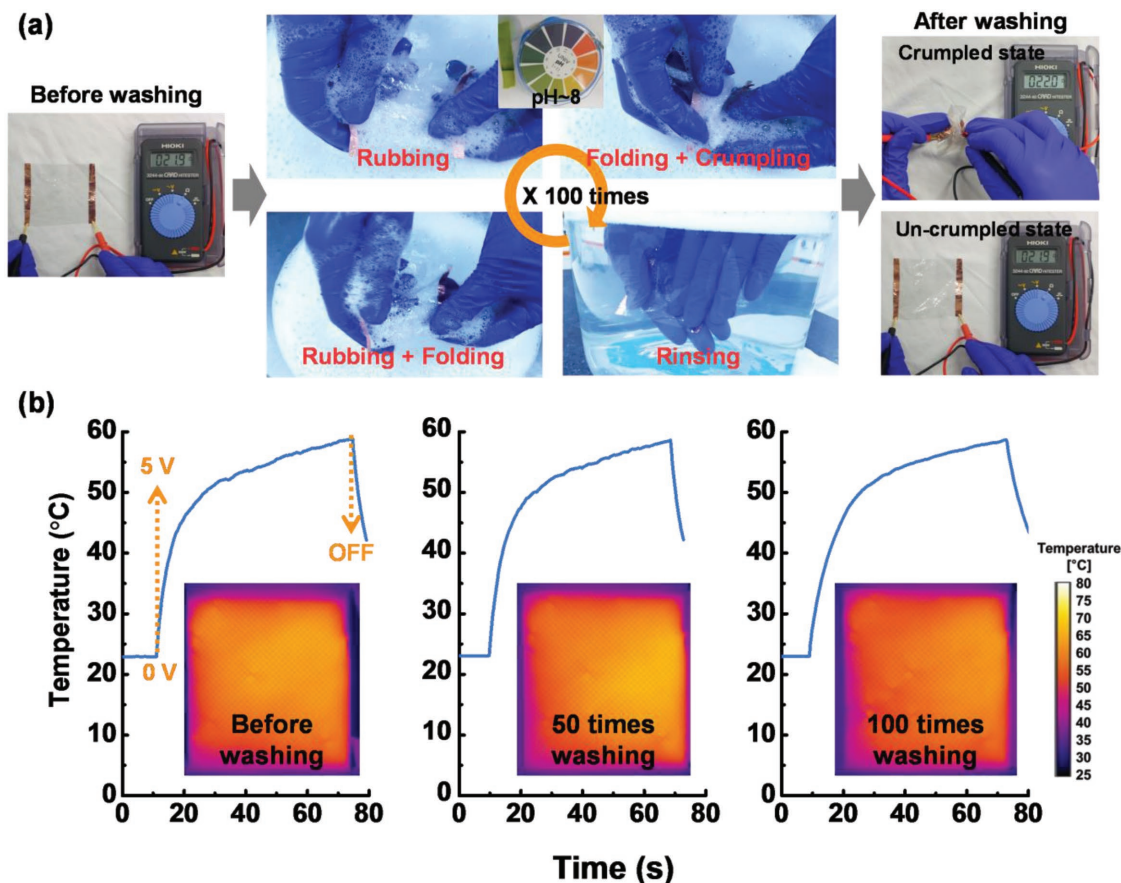


**Figure 4.** a) Photographs show the electrical properties of transparent conductive heater (TCH) before, during, and after washing. For realism, detergent was dissolved in water and then TCH was rubbed, folded, and crumpled in the prepared solution of pH  $\approx 8$ . b) Temperature evolution of the TCH at the applied voltage of 5 V as a function of washing times ranging from 0 to 100 times. The insets present IR images of the working TCH before washing and after 50 and 100 washing cycles.

of the mesh patterns (Figure S6, Supporting Information). Moreover, the temperature increased to approximately 60 °C by applying a constant DC bias of 5 V to the TCH and the uniform heating operation could be observed. After 50 and 100 repeated washing test cycles, the flexible TCH continued to exhibit stable heating. It is believed that our high-quality mesh and its fabrication process can contribute greatly to the development of extremely flexible and wearable electronic applications.

In summary, easily deformable highly soft rubber was applied to achieve conformal contact between the composite layer and the photomask in a selective photonic sintering-based simple patterning route. This approach allows us to reduce the maldistributed light intensity and augmented light diffraction, thereby leading to a defect-less, fine mesh pattern with a much higher uniformity ( $8.92 \pm 0.26 \Omega \text{ sq}^{-1}$ ), as compared to the conventional case without the rubber ( $801.8 \pm 978.5 \Omega \text{ sq}^{-1}$ ). In addition, it was confirmed that the patternability could be strongly dependent on the distribution of heat generated in the selectively IPL-irradiated film and better accurate patterns with desired performance could be obtained by adopting pattern design due to suppress inhomogeneous heat distribution. Moreover, instead of rubber support, applying a thin plastic substrate with low flexural rigidity could be helpful to fabricate pattern with high uniformity ( $8.14 \pm 0.23 \Omega \text{ sq}^{-1}$ ). Besides this effect, using a thin plastic substrate could allow the pattern to be positioned closer to the strain-free neutral mechanical plane. Owing to the strong interfacial adhesion between the mesh pattern and substrate, the mesh pattern could avoid the mechanical failures such as interfacial delamination, thereby exhibiting extraordinary flexibility. Finally, it was successfully demonstrated that a highly transparent heater with fine mesh patterns was fabricated on thin plastic substrate and this heater could be stable after 100 repeated washing test cycles, including being rubbed, folded, and crumpled in soapy water. The results of this study clearly show the high potential of our extremely flexible and highly durable transparent electrodes and their simple fabrication process to accelerate the ongoing development of low-cost and wearable electronics for real-life applications.

## Experimental Section

**Fabrication of AgNP–CNT Mesh:** AgNP–CNT ink was fabricated by the addition of the aqueous CNT-dispersion ink (8 wt%, Carbobyk, BYK) into a commercial ethanol-based AgNP ink (50 wt%, ROS 420, N&B). The CNT ink was added into the AgNP ink as 1.8 wt%, followed by ultrasonication for uniform dispersion. The obtained AgNP–CNT ink was deposited by spin-coating (4000 rpm/30 s) on PET (10 and 100  $\mu\text{m}$ , Teijin DuPont Films) substrates. The fabricated AgNP–CNT film was dried under ambient condition and patterned by use of a photonic sintering system (PulseForge 1300, Novacentrix) with a xenon flash lamp of broadband wavelength 200–1500 nm. The soft rubber utilized in the SLIP method was fabricated by mixing the prepolymer (A, Eco Flex 0030, SFX KOREA) and enhancer (B, Eco Flex 0030, SFX KOREA) at a 1:1 ratio with the thickness of  $\approx 5 \text{ mm}$  and dried naturally under ambient condition. The photomask, rubber, and AgNP–CNT film were fixed together by clamps and then the SLIP process was executed. The quartz photomask (comprising a patterned chrome masking layer) was designed with a transmittance of 95%, line width of 20  $\mu\text{m}$ , and the line spacing of 770  $\mu\text{m}$ . In the sintering process, the films were exposed to IPL irradiation with the same duration time of 1000  $\mu\text{s}$ . The wiping process was performed by a fabric soaked with ethanol to clear the

nonirradiated region. The error bar ( $y$ ) in Figures 1b and 3b was defined as the standard deviation of the measured line width of the mesh which was formulated as follows:

$$y = \sqrt{\frac{\sum (\omega - W)^2}{(n-1)}} \quad (3)$$

where  $\omega$ ,  $W$ , and  $n$  stand for the measured line width, the average line width and numbers of the measurement, respectively. To obtain the average line width of the mesh, four SEM images for every condition had been taken and the line width ( $\omega$ ) in every image ( $\omega_1$ ,  $\omega_2$ ,  $\omega_3$ , and  $\omega_4$ ,  $n = 4$ ) had been measured. Based on these data, the average line width ( $W$ ) could be calculated as  $(W_1 + W_2 + W_3 + W_4)/4$  and the error bars could be obtained.

**Simulation of Heat Conduction:** The heat conduction effect in the patterning after the selective IPL irradiation was simulated by using the commercial software ANSYS. For simplification and visualization, the quartz/chrome mask/Ag layer/PET film/rubber stack was established with the respective thicknesses of 260  $\mu\text{m}$ /600 nm/10  $\mu\text{m}$ /1 mm with one cross of the mask aperture size of 100  $\mu\text{m}$  and the sample size of  $4 \times 4 \text{ mm}^2$ . As the boundary conditions, the mask and the rubber were both assumed to be kept at a constant temperature (22 °C). To simulate the light irradiation, a heat flux of  $4 \times 10^7 \text{ W m}^{-2}$  for 1000  $\mu\text{s}$  was applied to the irradiated area of the film. To determine the thermal conductivity ( $\kappa_c$ ) of the AgNP–CNT composite, it was assumed that MWCNTs could not greatly affect the thermal conductivity of composite. Instead of CNTs, a polymer stabilizer (polyvinylpyrrolidone, PVP) could significantly decrease the thermal conduction of the composite. Considering this assumption, the thermal conductivity of the composite could be calculated by a theoretical model proposed by Lichtenecker, as follows:<sup>[41]</sup>

$$\log(\kappa_c) = \log(\kappa_{\text{PVP}}) \times (1 - \rho) + \rho \log(\kappa_{\text{Ag}}) \quad (4)$$

where  $\kappa_{\text{PVP}}$  and  $\rho$  represent the thermal conductivity of PVP ( $0.27 \text{ W m}^{-1} \text{ K}^{-1}$ ) and the volumetric fraction of AgNPs (0.95) in the composite, respectively. As a result, the thermal conductivity of the composite ( $\kappa_c$ ) was determined to be  $4.3 \text{ W m}^{-1} \text{ K}^{-1}$  and applied to the simulation.

**Characterizations of AgNP–CNT Mesh FTCE:** The morphology of the AgNP–CNT mesh film was observed by a confocal microscope (Optelicsr C130, Lasertec) and high-resolution FESEM (S4800, Hitachi Ltd.). The sheet resistance was measured with a noncontact eddy-current probe system (EC-80-P model, Napson Corp.). The transmittance of the FTCEs was measured by a UV–vis spectrophotometer (Lambda 750S model, PerkinElmer, Inc.) with a wavelength range of 300–1000 nm.

**Fabrication of TCH:** An AgNP–CNT mesh pattern of approximate dimensions  $60 \times 60 \text{ mm}^2$  was developed on a thin PET substrate (10  $\mu\text{m}$ ) by using the R-SLIP method. Both sides of the pattern were connected to a power supply unit (HM 7044, HAMEG Instruments) with copper conductive tape. The fabricated thermal heater had a series resistance of 21.9  $\Omega$ , as measured by a digital multimeter (Card HiTester 3244-60, HIOKI E.E. Corporation). The transmittance of the mesh heater was measured to be 95%. The washing test was conducted in soapy water by crumpling the ultraflexible TCH. The thermal heating performance was observed in real time by use of an IR camera (A600 series, FLIR Systems, Inc.)

## Supporting Information

Supporting Information is available from the Wiley Online Library or from the author.

## Acknowledgements

Z.Z. and K.W. contributed equally to this work. This work was supported by the Ministry of Trade, Industry & Energy (MOTIE, Korea), under the

Advanced Technology Center (ATC) Program (10067668), Technology Innovation Program (10052802), and government-funded Research Program of the Korea Institute of Machinery and Materials Technology Innovation Program (NK210D). It was also supported by a National Research Foundation of Korea (NRF) funded by the Korean government (MSIP) (2012R1A3A2026417, 2016M1A2A2940915).

Note: The Acknowledgements were updated on May 24, 2018 after initial online publication.

## Conflict of Interest

The authors declare no conflict of interest.

## Keywords

metal mesh transparent electrodes, patterning, photonic sintering, washable flexible heaters

Received: February 18, 2018  
Published online: April 17, 2018

- [1] S. Kim, H.-J. Kwon, S. Lee, H. Shim, Y. Chun, W. Choi, J. Kwack, D. Han, M. Song, S. Kim, S. Mohammadi, I. Kee, S. Y. Lee, *Adv. Mater.* **2011**, 23, 3511.
- [2] T. Sekitani, H. Nakajima, H. Maeda, T. Fukushima, T. Aida, K. Hata, T. Someya, *Nat. Mater.* **2009**, 8, 494.
- [3] T.-H. Han, Y. Lee, M.-R. Choi, S.-H. Woo, S. H. Bae, B. H. Hong, J.-H. Ahn, T.-W. Lee, *Nat. Photonics* **2012**, 6, 105.
- [4] T. Sekitani, T. Someya, *Mater. Today* **2011**, 14, 398.
- [5] Z. Yu, Q. Zhang, L. Li, Q. Chen, X. Niu, J. Liu, Q. Pei, *Adv. Mater.* **2011**, 23, 664.
- [6] R. V. Salvatierra, C. E. Cava, L. S. Roman, A. J. G. Zarbin, *Adv. Funct. Mater.* **2013**, 23, 1490.
- [7] X. Zhang, J. Zhang, J. Liu, E. M. J. Johansson, *Nanoscale* **2015**, 7, 11520.
- [8] Y. K. Seo, C. W. Joo, J. Lee, J. W. Han, N. S. Cho, K. T. Lim, S. Yu, M. H. Kang, C. Yun, B. H. Choi, Y. H. Kim, *Org. Electron.* **2017**, 42, 348.
- [9] P. C. Mahakul, K. Sa, B. Das, B. V. R. S. Subramaniam, S. Saha, B. Moharana, J. Raiguru, S. Dash, J. Mukherjee, P. Mahanandia, *J. Mater. Sci.* **2017**, 52, 5696.
- [10] X. Zhang, K. Aitola, C. Hägglund, A. Kaskela, M. B. Johansson, K. Sveinbjörnsson, E. I. Kauppinen, E. M. J. Johansson, *ChemSusChem* **2017**, 10, 434.
- [11] J. Yoon, H. Sung, G. Lee, W. Cho, N. Ahn, H. S. Jung, M. Choi, *Energy Environ. Sci.* **2017**, 10, 337.
- [12] Y.-S. Kim, E.-J. Lee, J.-T. Lee, D.-K. Hwang, W.-K. Choi, J.-Y. Kim, *RSC Adv.* **2016**, 6, 64428.
- [13] H. Dong, Z. Wu, Y. Jiang, W. Liu, X. Li, B. Jiao, W. Abbas, X. Hou, *ACS Appl. Mater. Interfaces* **2016**, 8, 31212.
- [14] Z. Zhong, K. Woo, I. Kim, H. Hwang, S. Kwon, Y.-M. Choi, Y. Lee, T.-M. Lee, K. Kim, J. Moon, *Nanoscale* **2016**, 8, 8995.
- [15] Z. Zhong, H. Lee, D. Kang, S. Kwon, Y.-M. Choi, I. Kim, K.-Y. Kim, Y. Lee, K. Woo, J. Moon, *ACS Nano* **2016**, 10, 7847.
- [16] H. Hwang, A. Kim, Z. Zhong, H.-C. Kwon, S. Jeong, J. Moon, *Adv. Funct. Mater.* **2016**, 26, 6545.
- [17] M. Kaltenbrunner, T. Sekitani, J. Reeder, T. Yokota, K. Kuribara, T. Tokuhara, M. Drack, R. Schwödiauer, I. Graz, S. B. Gogonea, S. Bauer, T. Someya, *Nature* **2013**, 499, 458.
- [18] M. S. White, M. Kaltenbrunner, E. D. Glowacki, K. Gutnichenko, G. Kettlgruber, I. Graz, S. Aazou, C. Ulbricht, D. A. M. Egbe, M. C. Miron, Z. Major, M. C. Scharber, T. Sekitani, T. Someya, S. Bauer, N. S. Sariciftci, *Nat. Photonics* **2013**, 7, 811.
- [19] S. Lee, A. Reuveny, J. Reeder, S. Lee, H. Jin, Q. Liu, T. Yokota, T. Sekitani, T. Isoyama, Y. Abe, Z. Suo, T. Someya, *Nat. Nanotechnol.* **2016**, 11, 472.
- [20] A. Miyamoto, S. Lee, N. F. Cooray, S. Lee, M. Mori, N. Matsuhisa, H. Jin, L. Yoda, T. Yokota, A. Itoh, M. Sekino, H. Kawasaki, T. Ebihara, M. Amagai, T. Someya, *Nat. Nanotechnol.* **2017**, 12, 907.
- [21] Z. Chen, J. W. F. To, C. Wang, Z. Lu, N. Liu, A. Chortos, L. Pan, F. Wei, Y. Cui, Z. Bao, *Adv. Energy Mater.* **2014**, 4, 1400207.
- [22] Y. Sameenoi, P. N. Nongkai, S. Nouanthavong, C. S. Henry, D. Nacapricha, *Analyst* **2014**, 139, 6580.
- [23] D.-Y. Cho, K. Eun, S.-H. Choa, H.-K. Kim, *Carbon* **2014**, 66, 530.
- [24] D. Y. Choi, H. W. Kang, H. J. Sung, S. S. Kim, *Nanoscale* **2013**, 5, 977.
- [25] J. H. Park, G.-T. Hwang, S. Kim, J. Seo, H.-J. Park, K. Yu, T.-S. Kim, K. J. Lee, *Adv. Mater.* **2017**, 29, 1603473.
- [26] S. Cho, S. Kang, A. Pandya, R. Shanker, Z. Khan, Y. Lee, J. Park, S. L. Craig, H. Ko, *ACS Nano* **2017**, 11, 4346.
- [27] E. B. Secor, S. Lim, H. Zhang, C. D. Frisbie, L. F. Francis, M. C. Hersam, *Adv. Mater.* **2014**, 26, 4533.
- [28] T. Choi, S. J. Kim, S. Park, T. Y. Hwang, Y. Jeon, B. H. Hong, *Nanoscale* **2015**, 7, 7138.
- [29] B.-Y. Wang, T.-H. Yoo, Y.-W. Song, D.-S. Lim, Y.-J. Oh, *ACS Appl. Mater. Interfaces* **2013**, 5, 4113.
- [30] S. Hong, J. Yeo, G. Kim, D. Kim, H. Lee, J. Kwon, H. Lee, P. Lee, S. H. Ko, *ACS Nano* **2013**, 7, 5024.
- [31] J. Noh, D. Yeom, C. Lim, H. Cha, J. Han, J. Kim, Y. Park, V. Subramanian, G. Cho, *IEEE Trans. Adv. Packag.* **2010**, 33, 275.
- [32] A. Mahajan, C. D. Frisbie, L. F. Francis, *ACS Appl. Mater. Interfaces* **2013**, 5, 4856.
- [33] I. Kim, K. Woo, Z. Zhong, E. Lee, D. Kang, S. Jeong, Y.-M. Choi, Y. Jang, S. Kwon, J. Moon, *ACS Appl. Mater. Interfaces* **2017**, 9, 6163.
- [34] G. Haacke, *J. Appl. Phys.* **1976**, 47, 4086.
- [35] B. Murali, D.-G. Kim, J.-W. Kang, J. Kim, *Phys. Status Solidi A* **2014**, 211, 1801.
- [36] Y. Galagan, J.-E. J. M. Rubingh, R. Andriessen, C.-C. Fan, P. W. M. Blom, S. C. Veenstra, J. M. Kroon, *Sol. Energy Mater. Sol. Cells* **2011**, 95, 1339.
- [37] I. Kim, S.-W. Kwak, Y. Ju, G.-Y. Park, T.-M. Lee, Y. Jang, Y.-M. Choi, D. Kang, *Thin Solid Films* **2015**, 580, 21.
- [38] W.-Y. Jin, R. T. Ginting, K.-J. Ko, J.-W. Kang, *Sci. Rep.* **2016**, 6, 36475.
- [39] J. Hu, L. Li, H. Lin, P. Zhang, W. Zhou, Z. Ma, *Opt. Mater. Express* **2013**, 3, 1313.
- [40] ASTM International, Standard Test Methods for Rating Adhesion by Tape Test, <http://www.astm.org>, <https://doi.org/10.1520/D3359-17>.
- [41] M. Jouni, A. Boudenne, G. Boiteux, V. Massardier, *Polym. Compos.* **2013**, 34, 778.